JGR Atmospheres

RESEARCH ARTICLE
10.1029/2022JD037563

# Future Projections of the El Niño—Southern Oscillation and Tropical Pacific Mean State in CMIP6

**Nathan E. Erickson[1] and Christina M. Patricola[1,2]**

[1]Department of Geological and Atmospheric Sciences, Iowa State University, Ames, IA, USA, [2]Lawrence Berkeley National Laboratory, Climate and Ecosystem Sciences Division, Berkeley, CA, USA

**Abstract** The El Niño—Southern Oscillation (ENSO) is an important mode of tropical Pacific atmosphere-ocean variability that drives teleconnections with weather and climate globally. However, prior studies using state-of-the-art climate models lack consensus regarding future ENSO projections and are often impacted by tropical Pacific sea-surface temperature (SST) biases. We used 173 simulations from 29 climate models participating in the Coupled Model Intercomparison Project, version 6 (CMIP6) to analyze model biases and future ENSO projections. We analyzed two ENSO indices, namely the ENSO Longitude Index (ELI), which measures zonal shifts in tropical Pacific deep convection and accounts for changes in background SST, and the Niño 3.4 index, which measures SST anomalies in the central-eastern equatorial Pacific. We found that the warm eastern tropical-subtropical Pacific SST bias typical of previous generations of climate models persists into many of the CMIP6 models. Future projections of ENSO shift toward more El Niño-like conditions based on ELI in 48% of simulations and 55% of models, in association with a future weakening of the zonal equatorial Pacific SST gradient. On the other hand, none of the models project a significant shift toward La Niña-like conditions. The standard deviation of the Niño 3.4 index indicates a lack of consensus on whether an increase or decrease in ENSO variability is expected in the future. Finally, we found a possible relationship between historical SST and low-level cloud cover biases in the ENSO region and future changes in ELI; however, this result may be impacted by limitations in data availability.

**Plain Language Summary** The El Niño—Southern Oscillation (ENSO) is an important pattern of tropical Pacific atmosphere-ocean variability that influences weather and climate globally. However, prior studies using state-of-the-art climate models lack consensus regarding future ENSO projections and are often impacted by tropical Pacific sea-surface temperature (SST) biases. We used 173 simulations from 29 global climate models to analyze model biases and future ENSO projections. We analyzed two ENSO indices, namely the ENSO Longitude Index (ELI), which measures zonal shifts in tropical Pacific deep convection, and the Niño 3.4 index, which measures SST anomalies in the central-eastern equatorial Pacific. We found that the warm eastern tropical-subtropical Pacific SST bias typical of previous generations of climate models persists into many of the current models. Future projections of ENSO shift toward more El Niño-like conditions based on ELI in the majority of models, in association with a future weakening of the zonal equatorial Pacific SST gradient. On the other hand, none of the models project a significant shift toward La Niña-like conditions. The standard deviation of the Niño 3.4 index indicates a lack of consensus on whether an increase or decrease in ENSO variability is expected in the future.

## 1. Introduction

The El Niño—Southern Oscillation (ENSO) is the dominant mode of interannual atmosphere-ocean variability. ENSO is characterized by sea-surface temperature (SST) variations in the eastern-to-central equatorial Pacific, with warm SST anomalies (SSTAs) during the positive phase, El Niño, and cool SSTAs during the negative phase, La Niña. ENSO peaks in boreal winter and has a periodicity of approximately 2–7 years (e.g., Philander, 1983; Rasmusson & Carpenter, 1982). Advanced knowledge about ENSO is useful for seasonal climate prediction and future climate projection, as ENSO drives teleconnections with many weather and climate extremes globally, including tropical cyclones and precipitation (e.g., Dai & Wigley, 2000; Gray, 1984; Hoerling, 2000; Kiladis & Diaz, 1989; Lin et al., 2020; McPhaden et al., 2006; Ropelewski & Halpert, 1987). The physical mechanism that drives ENSO's teleconnections is a zonal shift in tropical Pacific deep convection, which shifts eastward during El Niño and westward during La Niña. Such shifts in tropical deep convection can initiate tropical teleconnections

Nathan E. Erickson and Christina M. Patricola contributed equally to this work.

**Key Points:**

- We evaluated the ENSO Longitude Index (ELI), which measures zonal shifts in deep convection, and the Niño 3.4 index in 29 Coupled Model Intercomparison Project, version 6 models
- Most models are biased toward more El Niño-like conditions due to warm sea-surface temperature (SST) biases in the eastern tropical Pacific
- Based on ELI, 55% (none) of the models project a future shift toward more El Niño-like (La Niña-like) conditions, irrespective of SST bias

**Correspondence to:**
C. M. Patricola,
cmp28@iastate.edu

**Citation:**
Erickson, N. E., & Patricola, C. M. (2023). Future projections of the El Niño—Southern Oscillation and tropical Pacific mean state in CMIP6. *Journal of Geophysical Research: Atmospheres*, *128*, e2022JD037563. https://doi.org/10.1029/2022JD037563

Received 29 JUL 2022
Accepted 10 OCT 2023

**Author Contributions:**
**Conceptualization:** Christina M. Patricola
**Data curation:** Nathan E. Erickson, Christina M. Patricola
**Formal analysis:** Nathan E. Erickson, Christina M. Patricola
**Funding acquisition:** Christina M. Patricola
**Investigation:** Nathan E. Erickson
**Methodology:** Nathan E. Erickson, Christina M. Patricola
**Project Administration:** Christina M. Patricola

**Software:** Nathan E. Erickson, Christina M. Patricola
**Supervision:** Christina M. Patricola
**Visualization:** Nathan E. Erickson
**Writing – original draft:** Nathan E. Erickson, Christina M. Patricola
**Writing – review & editing:** Nathan E. Erickson, Christina M. Patricola

via a Walker Circulation response and mid-latitude teleconnections via a Rossby wave train response (Hoerling & Kumar, 2002; Horel & Wallace, 1981).

It is well known that not all El Niño events are alike, as the spatial patterns of SST warming can vary between events, often referred to as ENSO diversity (review papers by Capotondi, Wittenberg, et al., 2015; Timmermann et al., 2018). These spatial patterns are often referred to as "types" or "flavors" of ENSO; the two primary types are canonical and non-canonical El Niño events. In particular, canonical El Niño events are characterized by SST warming in the eastern tropical Pacific, often called "East Pacific El Niño" or "cold tongue El Niño," whereas non-canonical El Niño events are characterized by SST warming in the central tropical Pacific, often called "Central Pacific El Niño," "El Niño Modoki," or "warm pool El Niño" (Ashok et al., 2007). An increase in the frequency of Central Pacific El Niño events has been observed in recent decades (Lee & McPhaden, 2010). In addition to differences in spatial patterns of SSTAs, another notable difference between the two "types" of El Niño is that La Niña events tend to follow East Pacific El Niño events, but not Central Pacific El Niño events (Kug et al., 2009). Although the two primary El Niño SSTA patterns are often referred to as "types," some studies highlight that they are not distinct modes of variability, but are instead part of the same phenomenon (Takahashi et al., 2011). Regardless of possible differences in ENSO genesis mechanisms, a growing number of studies reveal the importance of ENSO diversity in modulating ENSO's teleconnections with extremes, including tropical cyclones and western US precipitation (e.g., Ashok et al., 2007; Patricola et al., 2016, 2018, 2020; Weng et al., 2007). The primary physical mechanism by which ENSO diversity modulates ENSO's teleconnections with extremes is related to the non-linear response in tropical Pacific deep convection to SST warming during El Niño. Differences in the location of SST warming, superimposed on the mean background state of the west Pacific warm pool and east Pacific cold tongue, can impact which tropical Pacific regions become favorable for deep convection, and therefore the extent to which deep convection shifts zonally. This then impacts the strength of the Walker Circulation response and the location of the Rossby wave train response (Johnson & Kosaka, 2016; Patricola et al., 2016, 2020) that makes remote conditions more or less favorable for weather and climate extremes regionally.

Despite the importance of ENSO for global extremes, it can be difficult to detect recent trends in ENSO and to project future changes in ENSO under global warming. One challenge in detecting trends in observations is that the record is short relative to the frequency of ENSO events. However, there is some evidence to support changes in ENSO in the recent historical period. For example, paleo-proxies of ENSO based on coral fossils suggest that ENSO variability is 25% stronger during the last 50 years compared with the pre-industrial period (Grothe et al., 2019). In addition, Linear Inverse Model simulations suggest that ENSO dynamics changed significantly in the late 1970's (Capotondi & Sardeshmukh, 2017).

Many studies have been performed attempting to project ENSO into the future, however, there is an overall lack of consensus. A review paper by Yeh et al. (2014) highlights substantial uncertainty in future changes in ENSO amplitude and spatial pattern. The difficulty in projecting future changes in ENSO amplitude and frequency has been attributed in part to the complexity of the processes that lead to ENSO growth and decay, including multiple positive and negative feedbacks (Collins et al., 2010). Even considering relatively recent climate model simulations from the Coupled Model Intercomparison Project, Phase 5 (CMIP5), some studies find no consensus on projections of future changes in ENSO (C. Chen et al., 2017), with a major source of uncertainty coming from the spatial pattern of tropical Pacific warming (Zheng et al., 2016). In particular, ENSO amplitude tends to increase (decrease) in models with enhanced (reduced) warming in the eastern equatorial Pacific (Zheng et al., 2016). Adding further complication to projecting ENSO is the possibility that future changes in ENSO amplitude may vary in time (Kim et al., 2014).

Despite much uncertainty around future ENSO projections, there are a few areas in which multiple studies find similar results. First, several studies indicate a possible increase in Central Pacific El Niño events relative to East Pacific El Niño events in the future, based on both the CMIP3 and CMIP5 models (Kim & Yu, 2012; Yeh et al., 2009). In addition, climate models tend to agree on future changes in the equatorial Pacific zonal SST gradient, with preferential warming in the eastern equatorial Pacific, representing a weakening of the equatorial Pacific zonal SST gradient (review paper by Cai, Santoso, et al. (2015), Fredriksen et al. (2020)). Finally, some studies find an increase in the frequency of ENSO events. Cai, Wang, et al. (2015) found almost a doubling in the frequency of La Niña events in the future, based on the Niño 4 index in the CMIP5 models, and Cai et al. (2014) found a doubling of extreme El Niño event frequency, based on rainfall in the eastern equatorial Pacific in the

CMIP3 and CMIP5 models. Similarly, a future increase in East Pacific SST variability was found in the CMIP5 models that capture the two types of ENSO (Cai et al., 2018), and among a subset of 11 CMIP6 models, 10 models project an increase in SST variance in the Niño 3.4 region (Fredriksen et al., 2020). El Niño and La Niña events are projected to become more frequent at the expense of neutral ENSO conditions in the Community Earth System Model-Large Ensemble (CESM-LENS) based on the ENSO Longitude Index (ELI); however, the Niño 3.4 index does not capture this response (Williams & Patricola, 2018).

There are multiple sources of uncertainty in future ENSO projections, including biases in climate models, for example, in the mean-state SST and trends in SST. Many generations of coupled global climate models (GCMs) have suffered from substantial biases in mean-state SST in the eastern tropical-subtropical Pacific (Richter, 2015; Zuidema et al., 2016), which overlaps with the region in which ENSO occurs. These SST biases can have contributions from the atmosphere (e.g., through errors in representing marine stratocumulus cloud decks and/or low-level coastal jets) and from the ocean (e.g., through errors in representing coastal upwelling, ocean eddies, and the thermocline). In addition to contributing to overall uncertainty in the projected climate of the tropical Pacific, biases in the mean-state SST and the thermocline can directly impact the representation of ENSO variability (e.g., Capotondi, Ham, et al., 2015) and have the potential to impact future projections of ENSO (Tang et al., 2021). In particular, Tang et al. (2021) found that removing common model biases in simulated Pacific SST results in a projected future Pacific SST change that is more La Niña-like, rather than El Niño-like. On top of mean-state SST biases, many models fail to reproduce observed trends in equatorial Pacific SST. In particular, Seager et al. (2019) found that although the equatorial Pacific zonal SST gradient has strengthened from 1958 to 2017, coupled models fail to capture this observed trend. Note that there is dependence on the time period considered for the trend, as some observational data sets for SST indicate a statistically significant cooling trend in eastern equatorial Pacific SST from 1900 to 2010, whereas the different products agree on a significant warming trend in the western equatorial Pacific (Deser et al., 2010).

In addition to model biases in representing the observed mean-state and trends in SST, biases have been documented in climate model representation of ENSO variability. One issue is that many climate models (CMIP3 and CMIP5) have biases in the spatial pattern of El Nino's warming, with warming maxima too far to the west (Bellenger et al., 2014; Capotondi, 2010; Capotondi et al., 2006; Guilyardi et al., 2009; Yang & Giese, 2013). Another problem related to the spatial pattern of ENSO is that most of the CMIP3 models fail to simulate the two primary observed types of El Niño, instead simulating only one type of El Niño (Ham & Kug, 2012). In addition, less than half of the CMIP3 models realistically simulate the observed intensity of the two types of ENSO (Yu & Kim, 2010). There have been some modest improvements in model representation of ENSO from CMIP3 to CMIP5, including better representation of ENSO's spatial patterns, amplitude, and lifecycle; however, the models still struggle to reproduce the observed intensity of East Pacific El Niño events (Bellenger et al., 2014; Kim & Yu, 2012). Several studies highlight the need for further improvements in climate model representation of ENSO, as realistic simulations of ENSO depend on both atmospheric and oceanic model components and their coupled feedbacks (Capotondi, Ham, et al., 2015; Guilyardi et al., 2009). Furthermore, there is great complexity to ENSO in terms of its spatial patterns, seasonal cycle, and genesis mechanisms. Indeed, it is difficult not only to simulate the climatology of observed ENSO characteristics, but also to predict ENSO events, such as the 2015/2016 El Niño (L'Heureux et al., 2017).

A second major source of uncertainty in future ENSO projections derives from the use of multiple ENSO indices (review paper by Capotondi, Wittenberg, et al. (2015)), many of which fail to characterize ENSO diversity. Among the most commonly used ENSO indices are those based on SSTAs averaged over various boxes within the equatorial Pacific, such as the Niño 3.4, Niño 3, Niño 4, and Niño 1 + 2 indices (Trenberth, 1997). Such indices can work well for a given climate state; however, it is challenging to apply them in a changing climate, which requires that the baseline SST climatology be re-defined over time, introducing artifacts into the time series. Furthermore, Niño 3.4 and related indices do not capture ENSO diversity, since they consider a fixed box; as a result, they do not capture the response of deep convection, which depends on SST rather than SSTA. To try to capture ENSO diversity, several indices have been developed to measure differences or gradients in SSTAs within the equatorial Pacific, including the Trans-Niño index (Trenberth & Stepaniak, 2001) and the El Niño Modoki Index (Ashok et al., 2007). In addition, there are several ENSO indices based on atmospheric variables, including the Southern Oscillation Index, which measures sea-level pressure differences between Tahiti and Darwin, Australia (Trenberth, 1984), an index based on outgoing longwave radiation anomalies in the eastern-central tropical Pacific (Chiodi & Harrison, 2013, 2015), and a precipitation-based index that measures rainfall averaged in

**Table 1**
*List of the 29 Coupled Model Intercomparison Project, Version 6 Models Analyzed, With the Number of Ensemble Members for Each Model*

| Model | Number of ensemble members with SST data available | Number of ensemble members with cloud cover data available |
|---|---|---|
| ACCESS-CM2 | 3 | 3 |
| ACCESS-ESM1-5 | 10 | 0 |
| AWI-CM-1-1-MR | 1 | 0 |
| BCC-CSM2-MR | 1 | 1 |
| CAMS-CSM1-0 | 2 | 0 |
| CanESM5 | 50 | 1 |
| CMCC-CM2-SR5 | 1 | 1 |
| CNRM-CM6-1 | 6 | 0 |
| CNRM-CM6-1-HR | 1 | 0 |
| CNRM-ESM2-1 | 5 | 0 |
| EC-Earth3 | 2 | 0 |
| EC-Earth3-Veg | 3 | 0 |
| FGOALS-f3-L | 1 | 1 |
| FGOALS-g3 | 4 | 1 |
| GFDL-CM4 | 1 | 0 |
| GFDL-ESM4 | 1 | 1 |
| GISS-E2-1-G | 7 | 0 |
| HadGEM3-GC31-LL | 4 | 0 |
| HadGEM3-GC31-MM | 4 | 0 |
| INM-CM4-8 | 1 | 0 |
| INM-CM5-0 | 1 | 0 |
| IPSL-CM6A-LR | 6 | 6 |
| MIROC6 | 50 | 9 |
| MIROC-ES2L | 1 | 0 |
| MPI-ESM1-HR | 2 | 1 |
| NESM3 | 2 | 1 |
| NorESM2-LM | 1 | 1 |
| NorESM2-MM | 1 | 1 |
| TaiESM1 | 1 | 1 |

*Note*. The total number of simulations with available SST data is 173 and the number with available cloud cover data is 29.

the Niño 3 region for El Niño (Cai et al., 2014). However, precipitation-based ENSO indices can overestimate future changes in El Niño due to precipitation change associated with global warming rather than ENSO; indeed, future ENSO projections depend strongly on the type of ENSO metric used, that is, SSTA-based or precipitation-based (Marjani et al., 2019). Similarly, future changes in El Niño events depend on whether the event is associated with extreme precipitation in the Niño 3 region or eastern equatorial Pacific SST warming, based on CMIP5 models (Wang et al., 2020). To address the various limitations of existing ENSO indices, the physically based ENSO Longitude Index (ELI) was developed (Williams & Patricola, 2018), which has several strengths including: it measures zonal shifts in tropical Pacific deep convection associated with ENSO, it captures ENSO diversity in a single metric, it accounts for changes in the background state SST associated with the seasonal cycle and climate change, and it explains teleconnections with tropical cyclone activity and global precipitation at least as well as Niño3.4 (Patricola et al., 2020, 2022; Williams & Patricola, 2018).

The purpose of our study is to better understand the behavior of ENSO and the tropical Pacific mean-state SST in a warming climate, in the context of climate model biases. We analyzed two ENSO indices, namely the ELI and Niño 3.4 index, in simulations from the multi-model ensemble of CMIP6 to address the following questions:

1. To what extent are CMIP6 models impacted by biases in tropical Pacific SST and ENSO representation?
2. What are the future projections of ENSO in the CMIP6 multi-model ensemble, based on ELI and the Niño 3.4 index?
3. What is the relationship between historical climate model biases and future projections of ENSO and the tropical Pacific mean-state SST?

This study is novel in evaluating future ENSO conditions using a physically based ENSO index that is capable of capturing ENSO diversity. In addition, we investigate the potential influence of climate model biases on future projections of ENSO and the Pacific mean state, which provides a better understanding of uncertainty.

## 2. Data

We used data from the CMIP6 multi-model ensemble (Eyring et al., 2016), which is organized under the World Climate Research Programme (WCRP). Using a multi-model ensemble accounts for a wide range of potential climate outcomes associated with the different climate sensitivities of each model. In total, we used SST data from 173 individual simulations from 29 CMIP6 climate models, and cloud cover data from 29 individual simulations from 14 CMIP6 climate models, which is all data available at the time of the study. Many of these models include multiple ensemble members, based on different physics schemes and initial conditions. We used the maximum number of ensemble members available, as large ensembles (consisting of 15–30 or more members) are best suited to quantify future changes in ENSO, given the substantial internal variability of the climate system (Maher et al., 2018; Zheng et al., 2018). A full list of the CMIP6 models used, including the number of ensemble members analyzed for each, can be found in Table 1.

For each model, we analyzed SST data from January 1850 through December 2100. For this data set, data from 1850 to 2014 was from the historical simulations, and data from 2015 to 2100 was from the future simulations based on the Shared Socioeconomic Pathway 5–8.5, which is generally considered to be a "worst-case scenario" for climate change and anthropogenic greenhouse gas emissions. Our analysis uses monthly SST data to calculate the ENSO indices described in the next section. Cloud cover data was similarly available from January 1850 through December 2100.

For observed SST data, we used the National Oceanic and Atmospheric Administration (NOAA) Extended Reconstructed SST Version 5 (ERSSTv5) monthly 2° × 2° SST (Huang et al., 2017a, 2017b), which covers January 1854 through the present. Observational cloud cover data was taken from the European Center for Medium-Range Weather Forecast Reanalysis, version 5 (ERA5) data set (ECMWF, 2019). The ERA5 reanalysis is on a 0.25° × 0.25° latitude-longitude grid and contains 37 vertical pressure levels. ERA5 cloud cover data is available from January 1980 through the present.

## 3. Methods

We used two indices to characterize ENSO in the ERSSTv5 observations and the CMIP6 simulations, namely, the Niño 3.4 index and ELI (Williams & Patricola, 2018). We use ELI because it is a physically based index that captures ENSO diversity in one metric and measures the zonal shifts in tropical Pacific deep convection that initiate teleconnections. Furthermore, ELI is well-suited for climate change studies, as it accounts for changes in background SST. We use ELI to measure the zonal shifts in average deep convection, rather than precipitation directly, as precipitation-based ENSO indices can overestimate future changes in El Niño due to precipitation change associated with global warming and the Clausius-Clapeyron relation (Marjani et al., 2019). The calculation of ELI follows a three-step process, with monthly SST as the sole input. First, the tropics-wide average SST is calculated in order to approximate a threshold for the presence of deep convection (Williams et al., 2009). This threshold temperature is calculated over the entire global tropics, defined as 5°N–5°S, with results insensitive to using this range or 20°N–20°S (Williams & Patricola, 2018). The second step involves applying a binary spatial mask to the tropics based on the threshold temperature. Grid points with SSTs equal to or warmer than the convective threshold are assumed to experience deep convection and are assigned a value of 1, whereas grid points with SSTs cooler than the threshold are assumed to have no deep convection and are assigned a value of 0. The final step in calculating ELI estimates the average longitude that experiences tropical Pacific deep convection, that is, the average longitude at which the local SST meets or exceeds the convective threshold SST. This step of the calculation is done in the tropics for the Pacific basin only. The monthly ELI is thus defined as this average longitude at which SSTs are greater than the threshold temperature for deep convection. We note that the calculation of ELI considers whether the convective threshold is exceeded, and ELI is not weighted by how much the convective threshold is exceeded; nevertheless, ELI explains the global responses of precipitation, temperature, and tropical cyclones at least as well as the Niño3.4 index (Balaguru et al., 2020; Magee & Kiem, 2020; Patricola et al., 2020, 2022; Williams & Patricola, 2018). There is a high correlation between the Niño3.4 index and ELI ($R = 0.86$ for the December–February (DJF) averages over 1870–2021), which is due to a strong relationship between the two indices for La Niña, neutral ENSO, and weak El Niño events (Figure 1a of Williams & Patricola, 2018); however, the correlation breaks down for strong El Niño events, which ELI is particularly well-suited to capture. In interpreting ELI, we note that ELI accounts for changes in ENSO associated with changes in ENSO variability and in the mean background SST state.

In addition to calculating ELI, we also calculate the Niño 3.4 index, which has been used as one of the standard indices for measuring ENSO over the last several decades (Li et al., 2010). However, its non-responsiveness to convective threshold effects causes it to poorly represent ENSO diversity. Niño 3.4 is calculated by taking the average SST anomaly over the region 5°N–5°S and 170°E − 120°E (Trenberth, 1997). The SST anomaly for a given year is calculated relative to the SST climatology for the surrounding 30 years, that is, 15 years prior through 15 years following. By using a running climatology, we attempt to avoid step changes in the Niño 3.4 index that can be introduced when using a climatology that is updated every decade. Calculating Niño 3.4 allows us to place our results within the context of many previous studies that used this index. In interpreting the Niño 3.4 index, we note that this index accounts for change in ENSO associated with changes in ENSO variability (e.g., ENSO amplitude and frequency), but unlike ELI, it does not account for changes in the mean background SST state. For this reason, the following analysis focuses on future change in the standard deviation of the Niño 3.4 index, which is a measure of ENSO variability, rather than future change in the mean of the Niño 3.4 index, which is expected to be minimal due to the construction of the index (i.e., the use of the running mean climatology).

## 4. Results

### 4.1. Validation of ENSO and Tropical Pacific Mean-State SST in Historical Climate Simulations

A primary focus of our study was to determine the prevalence and severity of biases simulated by the coupled climate models participating in CMIP6. We validate the historical simulations by comparing the observed and

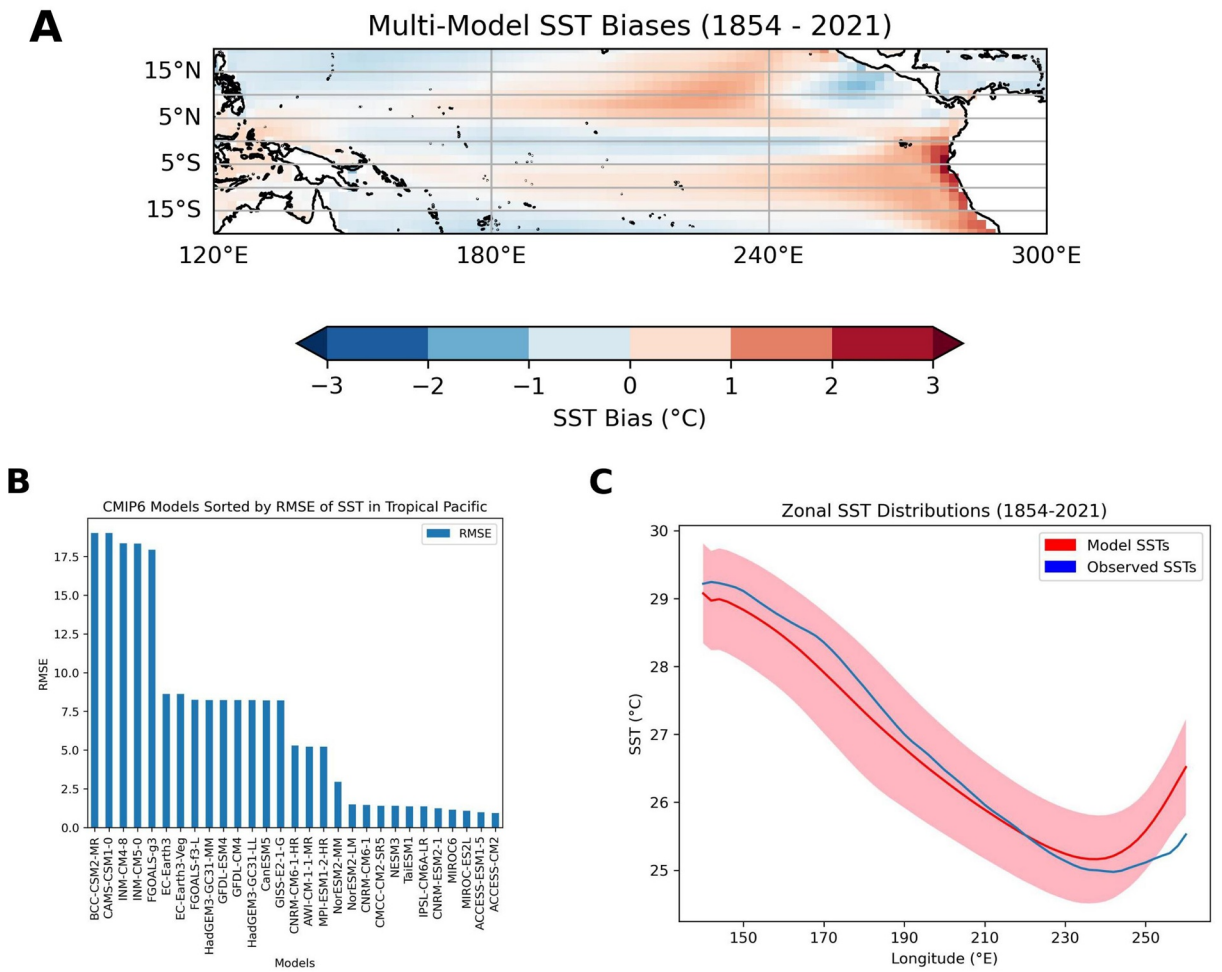


**Figure 1.** (a) Sea-surface temperature (SST) biases (°C) from the Coupled Model Intercomparison Project, version 6 (CMIP6) multi-model ensemble, averaged December–February (DJF) over 1854–2021. The SST biases were produced by regridding all CMIP6 models to the horizontal grid of the Extended Reconstructed SST Version 5 (ERSSTv5) data set, which was used as the baseline observed SST. Each model is weighted equally to produce the multi-model ensemble average bias (i.e., multiple ensemble members for a given model are averaged before creating the multi-model ensemble average). (b) CMIP6 models ranked according to their root mean square error for tropical Pacific SST, relative to the ERSSTv5 observations. (c) The zonal tropical Pacific SST distribution (°C), averaged over 5°N – 5°S and DJF over 1854–2021. The red line indicates the multi-model mean SST from CMIP6, with the standard deviation of modeled SSTs shaded in pink. Observed SST from ERSSTv5 is shown in blue.

simulated tropical Pacific SST climatology and ENSO distributions. Such validation gives us insight into the performance of the CMIP6 ensemble for simulating the historical statistics of ENSO events and allows us to interpret future ENSO projections in the context of model biases.

We begin by evaluating biases in the SST climatology over the tropical Pacific during ENSO's DJF peak for the CMIP6 models relative to the ERSSTv5 observations. Richter (2015) concluded that GCMs in the CMIP5 multi-model ensemble typically exhibit significantly warmer-than-observed SSTs in the ENSO region. The warm bias in the eastern tropical Pacific acts to weaken the zonal SST gradient in the tropical Pacific, which leads to a background SST that is biased toward more El Niño-like conditions. Figure 1a demonstrates that the SST bias commonly found in the eastern tropical Pacific in previous generations of models persists in CMIP6 and is most pronounced directly off the northwest coast of South America. Figure 1c shows the zonal SST distribution for the CMIP6 ensemble relative to the observations across the equatorial Pacific. The SST biases in the eastern tropical Pacific are largely robust across the multi-model ensemble (Figure 1c). While DJF averaged SSTs in the western tropical Pacific are captured somewhat well, substantial bias is evident in the eastern tropical Pacific; nearly every model simulates warmer than observed SST around 270°E (just off the coast of South America), and most of the models are 1–3°C warmer than observations on average in the far eastern Pacific. In addition, we calculated

the root mean square error (RMSE) of SST in the southeastern tropical Pacific for each CMIP6 model relative to observations (Figure 1b) to determine the average degree of bias in SST over the entire region of interest. For this analysis, we defined the southeastern tropical Pacific from 240°E to 290°E, and from 5°N to 5°S, where the most prominent SST biases are evident in Figure 1a. We use the RMSE later in the analysis to investigate possible relationships with future ENSO projections.

We next evaluate climate model biases in ENSO representation for all years in which SST observations were available (January 1854–December 2021), first using ELI and then the Niño 3.4 index, with both averaged during ENSO's DJF peak. Many of the models produced multiple ensemble members; thus, we assigned equal weight to each model by creating a single ELI or Niño 3.4 distribution for each model, made up of the ENSO index values for all ensemble members performed by the given model. We equally weighted each model because ensemble members from the same model are likely to be more similar to each other than simulations from different models. This method enables a more effective interpretation of the ENSO indices that will avoid over-emphasizing models that produced many ensemble members.

To classify models into different sub-groups based on representation of the Pacific mean state, we defined three divisions based on the DJF-averaged ELI over the period 1854–2021: those biased toward El Niño-like conditions (defined as a median ELI greater than or equal to 165°E), those with a roughly similar median ELI compared with observations (defined as a median ELI between 158°E and 165°E), and those biased toward La Niña-like conditions (defined as a median ELI less than 158°E). Divisions were created relative to the median observed ELI of about 158°E. Figures 2a–2c shows the DJF ELI distributions from 1854 to 2021 for each model, organized by the bias in median ELI. A clear pattern of bias is present within the CMIP6 ensemble. Of the 29 models analyzed, 17 (∼59%) exhibited an El Niño-like bias, 10 (∼34%) produced a median ELI similar to observed, and only 2 (∼7%) demonstrated a La Niña-like bias. The strong ELI-based bias toward El Niño-like conditions is consistent with the typical multi-model ensemble average mean-state SST biases in the tropical Pacific (Figure 1), with an average bias in southeastern tropical Pacific SST of 0.56°C and −0.66°C in the El Niño-like and La Niña-like models, respectively (Figure 2). Recall that ELI can capture such biases, as it can represent changes in both mean-state SST and in ENSO variability.

We next analyzed the distribution of DJF-averaged values of the Niño 3.4 index from 1854 to 2021. As with the ELI analysis, boxplots for a given model contain all available ensemble members for that model. Figures 2d–2f shows the distributions of Niño 3.4 for each CMIP6 model using the ELI-based bias groupings (El Niño-like, weakly biased, and La Niña-like). The Niño 3.4 distributions from the CMIP6 models do not demonstrate a clear pattern of bias in the median, even when grouped according to patterns of bias evident from ELI. We expect this result because the Niño 3.4 index quantifies SST anomalies relative to a background climatology that is updated over time (i.e., as the climate warms), so the Niño 3.4 index distribution should be centered near zero given a sufficient sample size. Although the Niño 3.4 index does not provide information about biases in mean-state SST, it does provide a useful basis to compare the tails of the distribution (i.e., strength of La Niña and El Niño events) between observations and the models. The models tend to produce a range of Niño 3.4 values that is either close to observed (i.e., weak bias in amplitude of ENSO events) or smaller than the observed range (i.e., biased toward low amplitude of ENSO events), with only a few models simulating values of the Niño 3.4 index that are more extreme than observed. The biases in the simulated extremes of the Niño 3.4 index appear to be independent of the ELI-based biases, indicating little connection between mean-state SST biases and biases in the amplitude of ENSO events.

### 4.2. Future Projections of ENSO and Tropical Pacific Mean-State SST

Given the interconnections between the mean-state and variability in the tropical Pacific, we begin our analysis of future projections by considering changes in the mean-state SST. Figure 3a shows the DJF-averaged multi-model SST change for 2050–2100 minus 1850–1900. The greatest future increase in SSTs is off the west coast of South America, centered just south of the equator. The entire tropical Pacific warms to some degree, but the spatial pattern of warming is highly variable in both the zonal and meridional directions. Along the equator, preferential warming is projected in the eastern Pacific, which would support more El Niño-like background conditions. To further examine future changes in the zonal SST gradient in the tropical Pacific, we considered SST changes for 2050–2100 minus 1850–1900 averaged over 5°N–5°S from each model (Figure 3b). While the detailed nature of warming differs between models, one consistent future climate response is stronger warming in the eastern tropical Pacific, which supports a future shift toward more El Niño-like conditions.

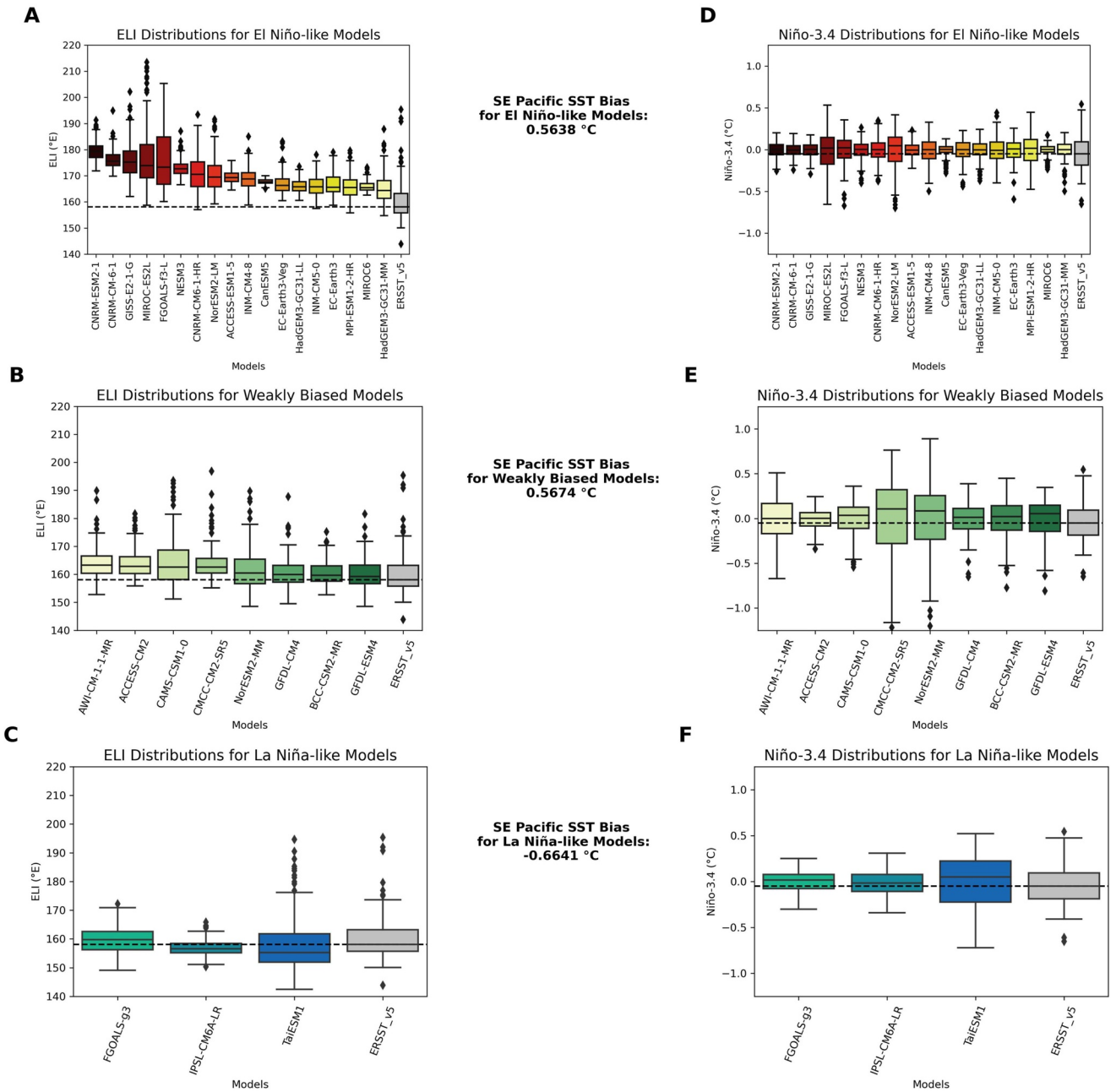


**Figure 2.** Box plots of December–February (DJF) averaged ENSO Longitude Index (ELI) (°E), over 1854–2021, from Extended Reconstructed SST Version 5 observations and from models with (a) El Niño-like ELI biases, (b) weak biases in median ELI, and (c) La Niña-like ELI biases, and (d)–(f) similar for DJF averaged Niño 3.4 (°C). The box plot for each model contains data between the first and third quartile of the distribution for each DJF value during 1854–2021 and for all ensemble members for that model. Whiskers extend to 1.5 times the interquartile range. Diamonds represent outlying points that fall outside the range of 1.5 times the interquartile range. The black dashed line denotes the median observed ELI/Niño 3.4, respectively. Average sea-surface temperature biases in the southeast tropical Pacific are indicated for each bias grouping.

Having shown that the zonal tropical Pacific SST gradient is generally projected to weaken in the future, consistent with Fredriksen et al. (2020), we next analyze future changes in both ENSO indices. Figure 4a shows the simulated temporal trends in ELI from 1850 to 2100, with a clear trend toward El Niño-like conditions (increasing values of ELI) in many of the simulations. This is consistent with the strong signal of a future weakening in the zonal SST gradient, that is, of preferential eastern Pacific SST warming from the historical period through the end of the 21st century.

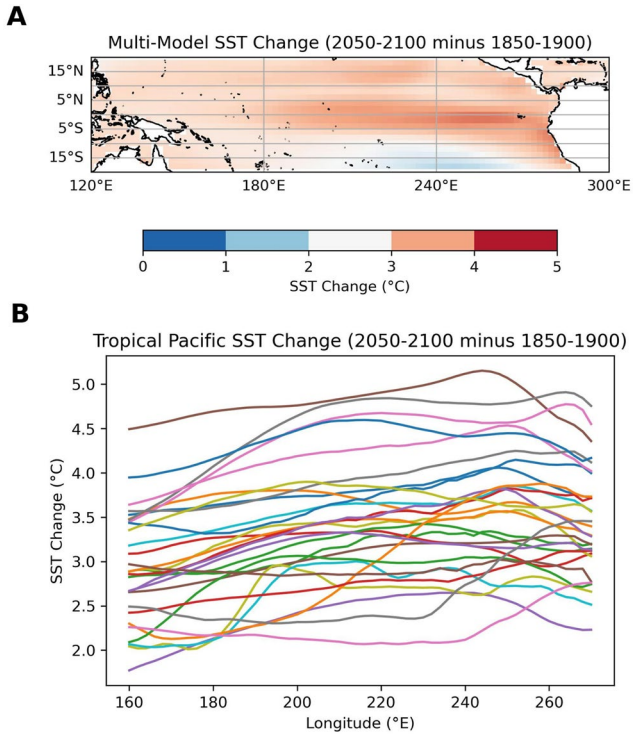


**Figure 3.** Future change (2050–2100 minus 1850–1900) in sea-surface temperature (SST) (°C) averaged December–February (a) from the Coupled Model Intercomparison Project, version 6 multi-model ensemble and (b) in the tropical Pacific zonal SST distribution (°C), averaged over 5°N–5°S. (a) As in Figure 1a, each model is weighted equally to produce the multi-model ensemble average SST change. (b) Each line represents the ensemble-mean from one model.

To fully grasp the significance of the trend toward more El Niño-like conditions, it is important to quantitatively measure the trend over time. We performed two-tailed T-tests to evaluate the significance of changes in ELI between two periods: the historical climate (1850–1900) and the future climate (2050–2100). We consider the changes using two approaches, first by considering all ensemble members of all models equally, then by considering each model equally regardless of its ensemble size. Table 2 shows the number of simulations that produced increases or decreases for each index, as well as those that produced statistically significant ($p < 0.05$) increases or decreases. Of the 173 simulations considered in our study, 134 (~77%) projected a shift toward increased ELI (i.e., more El Niño-like conditions) from historical to future, whereas only 39 simulations (~23%) projected an average decrease in ELI (i.e., more La Niña-like conditions). Additionally, 83 simulations (~48% of the entire data set) projected a statistically significant increase in ELI, whereas only one simulation indicated a statistically significant decrease in ELI.

To determine the robustness of these future ENSO projections, we next consider each model equally regardless of its ensemble size. We include this analysis to evaluate whether the future projections in the analysis above are weighted heavily by a few models that have many ensemble members. If almost all of the significant changes are produced by only a couple of the CMIP6 models, then the robustness of the predictions may be decreased. We found that 16 of the 29 CMIP6 models we used (or 55% of models used) had at least 50% of their ensemble members project a statistically significant increase in ELI; of these 16 models, nine had multiple ensemble members. On the other hand, none of the models had at least 50% of their ensemble members project a statistically significant decrease in ELI. This result strengthens the robustness of the future ENSO projections, as it indicates that 55% of the models, some of which contain multiple ensemble members, produce a consensus regarding a future shift toward more El Niño-like conditions.

We next evaluate future changes in ENSO using the Niño 3.4 index. Since the Niño 3.4 index removes the running mean climatology, we do not expect to find substantial changes in the mean over time. Indeed, due to the construction of the index, changes in the average Niño 3.4 index are insignificant between the future and historical climates. Figure 4b shows no clear trend in the Niño 3.4 index from 1850 to 2100. T-tests were performed on the Niño 3.4 distributions in the same manner as they were for ELI, and no simulations produced statistically significant future changes in Niño 3.4 (Table 2). Instead, the Niño 3.4 index is useful for evaluating changes in the amplitude of ENSO events, which can be quantified using the standard deviation of the Niño 3.4 index, calculated over each 30-year period centered on the given year. Figure 4c shows the trend of the standard deviation of Niño 3.4 with time, and Table 2 summarizes the projected changes in the standard deviation of Niño 3.4. Overall, 103 simulations produced a significant change in the standard deviation of Niño 3.4, with 72 (42%) projecting a significant increase in the standard deviation and 31 (18%) projecting a significant decrease in the standard deviation. Although the overall interannual variability in ENSO according to Niño 3.4 is projected to change in the future climate in many of the simulations, there is a lack of consensus on whether an increase or decrease in ENSO variability is expected.

### 4.3. Influence of Model Bias on Future Projections of ENSO and Tropical Pacific Mean-State

Now that we have evaluated biases in the mean-state tropical Pacific SST and in the distribution of ENSO, and analyzed future ENSO projections, we explore whether there is any relationship between the two. Given that no climate model can perfectly represent the historical climate, it is useful to understand model biases so that we can better gauge uncertainties in future projections. Figure 5 shows paired boxplots of ELI distributions for the three ELI-based bias groups introduced in Section 4.1, with the historical and future distributions side-by-side for

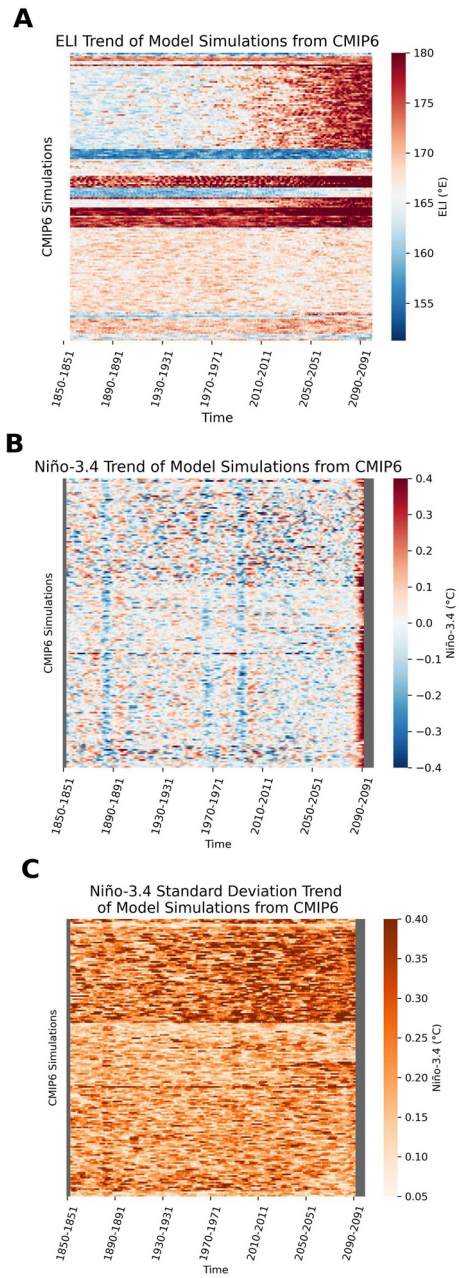


**Figure 4.** Heatmap displaying trends in the December–February averaged (a) ENSO Longitude Index (°E), (b) the Niño 3.4 index (°C), and (c) the standard deviation of the Niño 3.4 index (°C) over time for all available climate models and ensemble members in the Coupled Model Intercomparison Project, version 6 simulations (i.e., each horizontal stripe represents one ensemble member of a climate model). Lower values in blues indicate (a) La Niña-like conditions, (b) La Niña events, and (c) a decrease in El Niño—Southern Oscillation (ENSO) variability; higher values in reds indicate (a) El Niño-like conditions, (b) El Niño events, and (c) and increase in ENSO variability. (a) The color bar is bounded by 150°E and 180°E; values less than 150°E indicate an extremely strong La Niña event, while values greater than 180°E indicate an extremely strong El Niño event. (b), (c) The Niño 3.4 index only runs through 2085, as opposed to 2100, to prevent the appearance of artificial warming trends caused by the rolling climatology at the start and end of the data record. Each of these figures is visually "smoothed" to show the 7-year average value of each index to improve readability.

each model. Generally, a translation of the distribution suggests a changing tropical Pacific zonal SST gradient, whereas a stretching/compression of the distribution indicates an increase/decrease in ENSO events (i.e., greater or fewer number of extreme El Niño and La Niña events). Overall, the primary difference projected between the historical and future climates is a translation of the distribution, consistent with the substantial future decrease in the tropical Pacific zonal SST gradient presented in Section 4.2.

To further study the relationship between climate model biases and projected changes, we examined correlations between DJF averaged biases in the ENSO indices, in SST, and in cloud cover (included because it is commonly associated with SST biases in our region of interest), and the projected changes in the ENSO indices (Figure 6) using all models and ensemble members available at the time of this study. Biases in the ENSO metrics are derived from the results presented in Section 4.1. SST and cloud cover biases are calculated over the southeastern tropical Pacific, bounded by 5°N–5°S and 240°E − 290°E. Climate model biases in cloud cover in the southeastern tropical Pacific are primarily associated with low-level stratocumulus (Richter, 2015); therefore, we analyze cloud cover at levels below 500 mb. Overall, the linear correlations between model biases and projected ENSO changes are generally weak (Figure 6), except for the relationship between mean SST bias in the southeast tropical Pacific and the mean projected change in ELI (Figure 6c; Pearson coefficient of 0.548) and the relationship between RMSE of tropical Pacific SST and the mean projected change in ELI (Figure 6g; Pearson coefficient of 0.51). This indicates that projected changes in ELI may be influenced by the mean-state SST bias in the historical climate. However, it is important to note that some models have many ensembles members, whereas others do not, leading to the possibility that this result is strongly influenced by a small number of models that have many ensemble members.

Therefore, we performed similar analysis using the ensemble mean from each available model to investigate whether the correlations were caused by a small number of models that have many ensemble members (Figure 7). This analysis lends further support for a portion of the results in Figure 6, including a negligible relationship between historical ELI bias and projected future ELI change and a moderate negative correlation between historical Niño 3.4 standard deviation bias and projected future Niño 3.4 standard deviation change, while indicating that the relationship between tropical Pacific SST biases and future change in ELI may be highly influenced by models with many ensemble members. Additionally, there is a moderate negative correlation (Pearson coefficient of −0.527) between cloud bias and projected future ELI change (Figure 7e); however, this result should be taken with caution due to relatively few simulations with available cloud cover data.

Finally, we also analyzed the relationship between historical bias in the developing ENSO seasons—boreal summer, (June, July, and August (JJA)), as well as boreal autumn (September, October, and November (SON)) and projected future change in the peak ENSO season, boreal winter. Figure 8 shows the relationship between mean-state SST bias in the historical climate for boreal summer/autumn and projected future change in ELI for boreal winter. A strong positive correlation (Pearson coefficient of 0.867 for JJA/0.824 for SON) is evident between historical climate SST bias in the developing ENSO seasons and future change in peak season ELI. Minimal correlation was present between the other bias metrics evaluated and future change in peak season ENSO indices. Thus, while some dependence on historical bias is suggested

**Table 2**
*The Number of Simulations Indicating Increases and Statistically Significant Increases ($p < 0.05$), as Well as Decreases and Statistically Significant Decreases ($p < 0.05$) in Mean ENSO Longitude Index and Mean and Standard Deviation of the Niño 3.4 From the Historical Climate (1850–1900) to the Future Climate (2050–2100)*

| ENSO index | Increase | Significant increase | Decrease | Significant decrease |
|---|---|---|---|---|
| *ELI* | 134 (77%) | 83 (48%) | 39 (23%) | 1 (1%) |
| *Niño 3.4* | 152 (88%) | 0 (0%) | 21 (12%) | 0 (0%) |
| *Niño 3.4 Standard Deviation* | 116 (67%) | 72 (42%) | 57 (33%) | 31 (18%) |

*Note*. Numbers in parentheses indicate the percent of simulations out of the total 173 considered that projected the given change.

for the future projections, further analysis must be done to clarify if the projections and bias are related quantitatively; we show this analysis next. Here, we examine the proportions of simulations in each bias grouping that project statistically significant changes in ELI. Table 3 shows the number of simulations in each ELI-based bias grouping, as well as the numbers and percentages indicating statistically significant increases in future ELI from each grouping. The vast majority of simulations (~83%) fell into the El Niño-like bias grouping (145 of 173 simulations). Of these, ~48% (70 of 145 simulations) projected statistically significant increases in ELI. Meanwhile, the weakly biased group had 21 simulations, of which 14 (66%) projected a statistically significant increase in future ELI. The sample size in the La Niña-like biased group is very small, with only seven simulations. The percent of simulations projecting a significant future increase in ELI does not vary substantially between models with an El Niño-like bias and models with weak ELI-based bias, suggesting little dependence of future ENSO projections on such biases.

## 5. Discussion and Conclusions

Despite ENSO's importance for driving teleconnections with weather and climate globally, there has been a lack of consensus regarding future ENSO projections. Two major challenges that make it difficult to project future ENSO conditions include model biases and, until recently, the lack of an ENSO index that can capture the diversity of El Niño's spatial variations. To work toward solving this problem, we investigated three questions using the CMIP6 multi-model ensemble: First, what is the prevalence and severity of model biases in tropical Pacific mean-state SST and ENSO; second, how are ENSO and the tropical Pacific mean-state SST projected to change into the future; and finally, what is the relationship between climate model biases and future ENSO projections? We addressed these questions by analyzing 173 simulations from 29 CMIP6 models. We evaluated two ENSO indices: (a) ELI, which tracks the zonal shifts in tropical Pacific deep convection that drive teleconnections with global weather, captures ENSO diversity, and accounts for changes in background SST associated with climate change and (b) the Niño 3.4 index, which is based on SST anomalies in a fixed region and therefore fails to capture ENSO diversity.

**Table 3**
*The Number of Simulations Projecting Increases (i.e., Shifts Toward More El Niño-Like Conditions) and Statistically Significant Increases ($p < 0.05$; i.e., Statistically Significant Shifts Toward More El Niño-Like Conditions) in ENSO Longitude Index From the Historical Climate (1850–1900) to the Future Climate (2050–2100)*

| Group (ELI-based bias) | Number of simulations in group | Number of simulations with significant increase in ELI |
|---|---|---|
| El Niño-like | 145 | 70 (48%) |
| Weakly Biased | 21 | 14 (66%) |
| La Niña-like | 7 | 0 (0%) |

*Note*. Numbers in parentheses indicate the percent of simulations out of the total within a given group that projected a significant increase in ELI.

We found that the biases typical of previous generations of climate models (e.g., Richter, 2015; Zuidema et al., 2016) remain prevalent in the CMIP6 ensemble. In particular, the vast majority of models simulate a warm SST bias in the eastern tropical-subtropical Pacific, which results in a significant portion of the models (~59%, or 17 of 29 models) biased toward El Niño-like conditions, based on median values of ELI. Only 10 of the 29 models (~34%) were weakly biased according to median ELI, and even fewer, 2 of the 29 models (~7%), demonstrated La Niña-like biases. Regarding future ENSO projections, we found that a large majority (~77%) of CMIP6 simulations projected a future shift toward more El Niño-like conditions, based on ELI, with roughly half of the simulations (48%) projecting a statistically significant increase. Furthermore, 16 of the 29 CMIP6 models (~55%) projected a future shift toward more El Niño-like conditions, whereas none of the models projected a future shift toward more La Niña-like conditions, demonstrating that the projections are quite robust. Importantly, these future ENSO projections did not depend on model biases in ELI. The Niño 3.4 index, which by

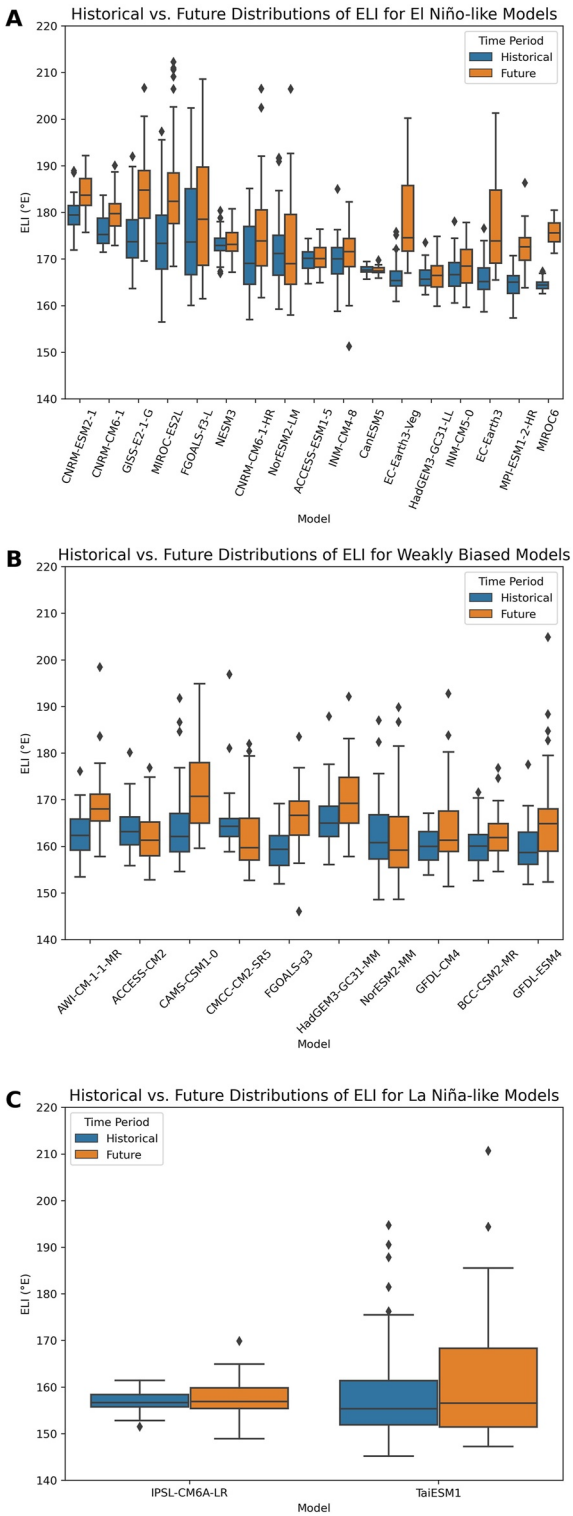


**Figure 5.** Box plots comparing historical (1850–1900; blue) and future (2050–2100; orange) climate distributions of December–February averaged ENSO Longitude Index (ELI) (°E) for models with (a) El Niño-like ELI biases, (b) weak median biases in ELI, and (c) La Niña-like ELI biases.

definition does not account for changes in background SST, unsurprisingly showed no coherent change into the future. However, the projected changes in the standard deviation of Niño 3.4 between the historical and future climates suggest a possible future change in ENSO variability, although there is a lack of consensus in the models regarding the sign of the change, with 42% (18%) of simulations projecting a significant increase (decrease) in ENSO variability in the future.

Altogether, these results provide strong evidence of climate change's effect on ENSO; based on the comparisons between historical and future ELI, we expect a future shift toward more El Nino-like conditions to manifest through a change in the mean-state SST, particularly a future weakening of the zonal SST gradient. Regarding the connection between model biases and future ENSO projections, we found a moderate correlation between historical climate SST and low-level cloud cover biases in the southeastern tropical Pacific and the projected future change in ELI. This result suggests that there may be a relationship between historical bias and projected future shifts toward El Niño-like conditions; however, an important caveat is that these results are heavily influenced by a small number of climate models with many ensemble members for SST and by limited data availability for cloud cover. This raises the possibility that any substantial historical bias relating to ENSO may significantly alter our future projections of ENSO, highlighting the need for further work to remedy persistent climate model biases. It would also be useful to consider how climate model biases during ENSO's development and decay stages may influence future projections of ENSO in future work.

Useful contributions for potential future studies include investigating the physical mechanisms that contribute to biases in ENSO; for example, through the processes that play a role in the Bjerknes feedback (Bjerknes, 1969). This includes exploring the models for potential systematic errors in simulating atmospheric factors such as trade winds, the westerly wind bursts that can be important for ENSO (e.g., D. Chen et al., 2015; Fedorov, 2002; Fedorov et al., 2015; Harrison & Giese, 1991; Harrison & Luther, 1990; Hu et al., 2014; Lengaigne et al., 2004; Seiki et al., 2011; Yu & Fedorov, 2020), the sensitivity of the surface wind response to SSTAs (van Oldenborgh et al., 2005), and deep convection (e.g., Guilyardi et al., 2009; Lloyd et al., 2009; Ma & Jiang, 2021; Neale et al., 2008; Watanabe et al., 2011; Wu et al., 2007). In addition, errors can also be associated with oceanic factors, for example, the simulated thermocline and downwelling Kelvin waves triggered by westerly wind bursts (e.g., Jin et al., 2006; Kim & Jin, 2011; McPhaden et al., 1988; Picaut & Delcroix, 1995). Given that coupled atmosphere-ocean feedbacks can potentially amplify errors within a given model component, mechanistic experiments with atmosphere-only, ocean-only, and coupled atmosphere-ocean models may be useful toward untangling the challenging problem of identifying and improving the sources of errors in simulations of ENSO.

A significant novel component of this study is its simultaneous usage of multiple indices for characterizing ENSO. We are unaware of other studies that compare ENSO projections from ELI with other indices such as Niño 3.4 to gain different insights from each. This study confirms the urgent need to supplement traditional ENSO indices such as Niño 3.4 with more physically based indices such as ELI. The Niño 3.4 index is able to capture the basic oscillatory nature of ENSO. However, it is not designed to capture changes

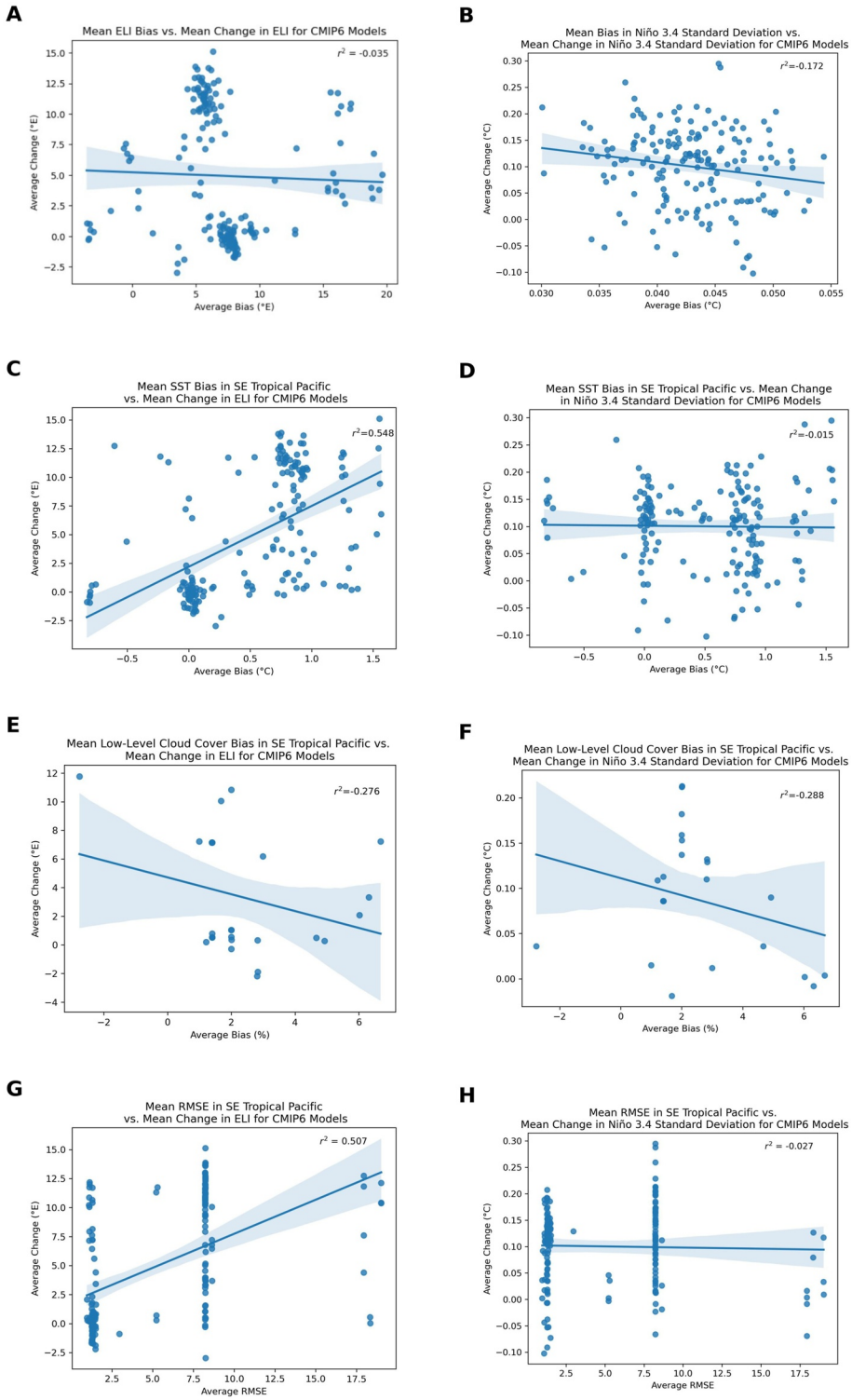


**Figure 6.** Scatterplots showing (a) mean bias in ENSO Longitude Index (ELI) versus mean future change in ELI, (b) bias in Niño 3.4 standard deviation versus mean future change in Niño 3.4 standard deviation, (c) mean sea-surface temperature (SST) bias in SE tropical Pacific versus mean future change in ELI, (d) mean SST bias in SE tropical Pacific versus mean future change in Niño 3.4 standard deviation, (e) mean low-level cloud cover bias in SE tropical Pacific versus mean future change in ELI, (f) mean low-level cloud cover bias versus mean future change in Niño 3.4 standard deviation, (g) mean root mean square error (RMSE) versus mean future change in ELI, and (h) mean RMSE versus mean future change in Niño 3.4 standard deviation for all available climate models and all ensemble members in Coupled Model Intercomparison Project, version 6. All data are averaged December–February. Each point represents one ensemble member of a climate model. The linear regression, along with the 95% confidence interval, is also plotted for each relationship. The Pearson coefficient for each relationship is shown at top right.

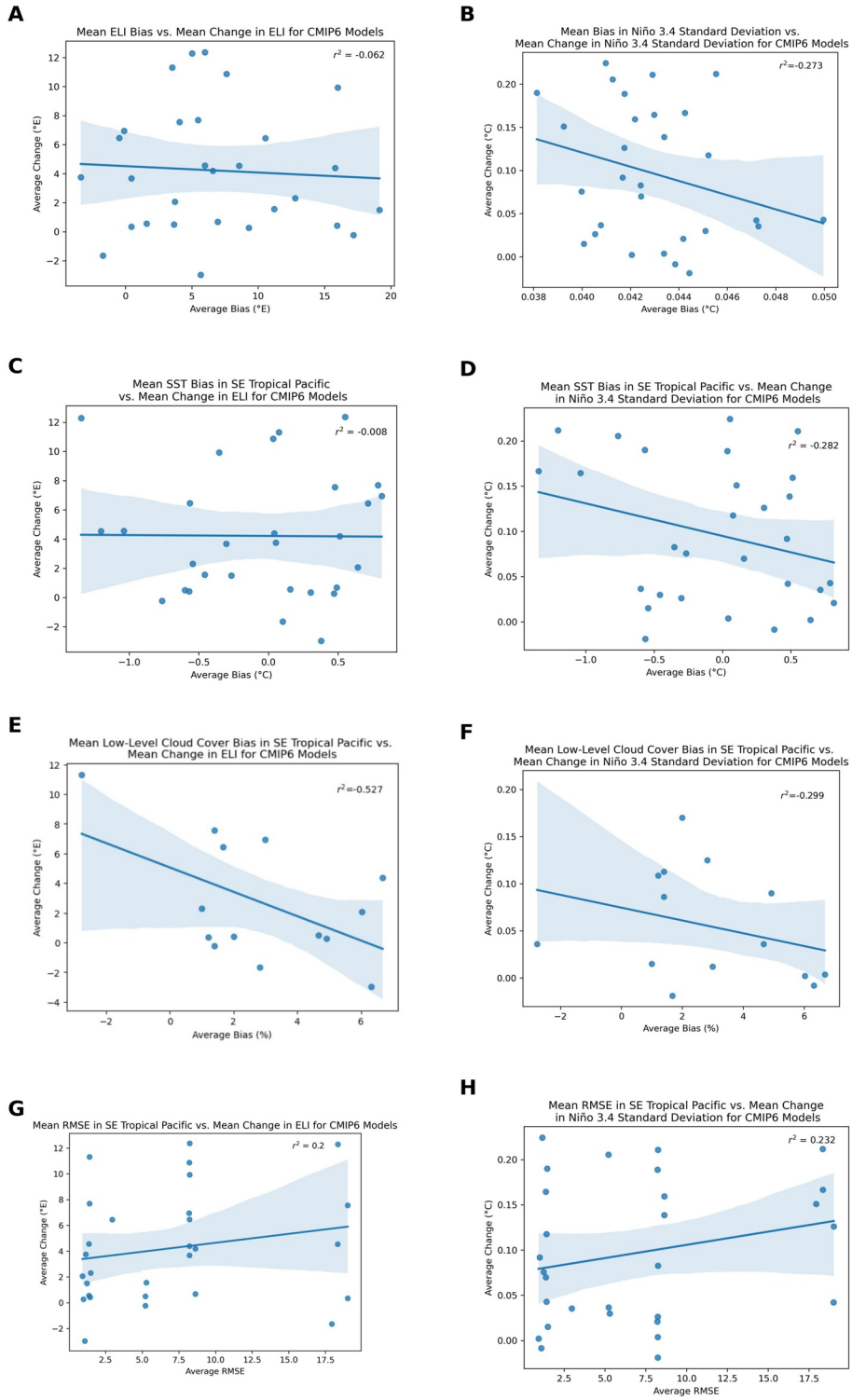


**Figure 7.** Analogous to Figure 6, but instead each point represents the ensemble mean, as opposed to showing all ensemble members, each as one point.

in ENSO diversity between historical and future climates, and it is not able to provide information about the climate model SST biases important for ENSO. To most effectively interpret future ENSO projections, we need to simultaneously uncover climate model biases and project future ENSO changes associated with changes in

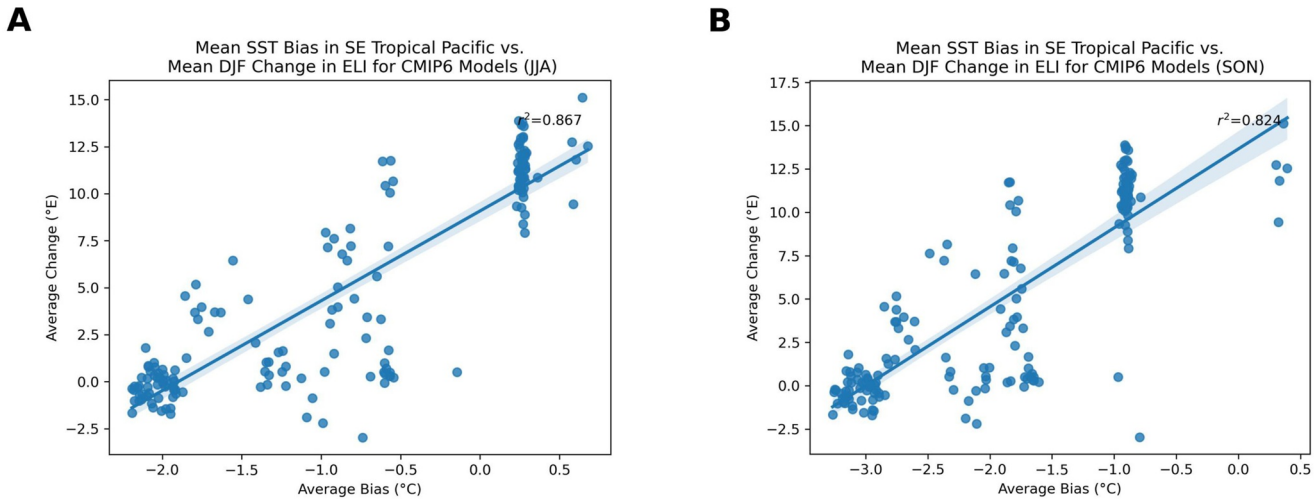


**Figure 8.** Scatterplots showing mean sea-surface temperature bias in the SE tropical Pacific for (a) June, July, and August and (b) September, October, and November, versus the mean future change in December–February ENSO Longitude Index. Each point represents one ensemble member of a climate model. The linear regression, along with the 95% confidence interval, is also plotted for each relationship. The Pearson coefficient for each relationship is shown at top right.

mean-state SST and SST variability. The Niño 3.4 index is limited in this respect, but ELI can accomplish both. Therefore, one significant finding from our study pertains to the appropriate usage for each of these indices. Niño 3.4 is effective at capturing departures in SST from a climatological average, which works well to diagnose future changes in ENSO variability, whereas ELI is effective for diagnosing change in ENSO associated with both mean climate change and change in variability, as it can discern shifts in background conditions over time and illuminate biases between models and observations. The broad utility of ELI is further apparent in considering the physical mechanisms by which ENSO influences global weather. In particular, the projected future shift toward more El Niño-like conditions revealed by ELI indicates an eastward shift in tropical Pacific deep convection in the future. It is this zonal shift in deep convection that likewise affects the Walker circulation and the Rossby wave train responses to ENSO, and therefore may provide critical information for potential changes in extreme weather and climate events worldwide.

## Data Availability Statement

The authors would like to acknowledge the WCRP for compiling the CMIP6 model data, which can be found at https://esgf-node.llnl.gov/projects/cmip6/. We acknowledge the NOAA Physical Sciences Laboratory for creating and maintaining the ERSSTv5 data set (Huang et al., 2017a, 2017b), which can be found at https://psl.noaa.gov/data/gridded/data.noaa.ersst.v5.html. Figures for the project were made with the Python packages Matplotlib, (Caswell et al., 2022), Seaborn (Waskom, 2021) and Xarray (Hoyer et al., 2022).

**Acknowledgments**
This material is based upon work supported by the Iowa State University, College of Liberal Arts and Sciences (LAS) Dean's High Impact Undergraduate Research Award, by the U.S. Department of Energy, Office of Science, Office of Biological and Environmental Research, Climate and Environmental Sciences Division, Regional and Global Model Analysis Program, and by the National Science Foundation under Grant AGS-2043272. We would like to thank four anonymous reviewers for their constructive comments that have helped improve the manuscript. Open access funding provided by the Iowa State University Library.

## References

Ashok, K., Behera, S. K., Rao, S. A., Weng, H., & Yamagata, T. (2007). El Niño Modoki and its possible teleconnection. *Journal of Geophysical Research*, *112*(C11), 505. https://doi.org/10.1029/2006JC003798

Balaguru, K., Patricola, C. M., Hagos, S. M., Leung, L. R., & Dong, L. (2020). Enhanced predictability of eastern North Pacific tropical cyclone activity using the ENSO longitude index. *Geophysical Research Letters*, *47*(16), e2020GL088849. https://doi.org/10.1029/2020gl088849

Bellenger, H., Guilyardi, E., Leloup, J., Lengaigne, M., & Vialard, J. (2014). ENSO representation in climate models: From CMIP3 to CMIP5. *Climate Dynamics*, *42*(7–8), 1999–2018. https://doi.org/10.1007/s00382-013-1783-z

Bjerknes, J. (1969). Atmospheric teleconnections from the equatorial Pacific. *Monthly Weather Review*, *97*(3), 163–172. https://doi.org/10.1175/1520-0493(1969)097,0163:ATFTEP.2.3.CO;2

Cai, W., Borlace, S., Lengaigne, M., van Rensch, P., Collins, M., Vecchi, G., et al. (2014). Increasing frequency of extreme El Niño events due to greenhouse warming. *Nature Climate Change*, *4*(2), 111–116. https://doi.org/10.1038/nclimate2100

Cai, W., Santoso, A., Wang, G., Yeh, S.-W., An, S.-I., Cobb, K. M., et al. (2015). ENSO and greenhouse warming. *Nature Climate Change*, *5*(9), 849–859. https://doi.org/10.1038/nclimate2743

Cai, W., Wang, G., Dewitte, B., Wu, L., Santoso, A., Takahashi, K., et al. (2018). Increased variability of eastern Pacific El Niño under greenhouse warming. *Nature*, *564*(7735), 201–206. https://doi.org/10.1038/s41586-018-0776-9

Cai, W., Wang, G., Santoso, A., McPhaden, M. J., Wu, L., Jin, F.-F., et al. (2015a). Increased frequency of extreme La Niña events under greenhouse warming. *Nature Climate Change*, *5*(2), 132–137. https://doi.org/10.1038/nclimate2492

Capotondi, A. (2010). El Niño–Southern Oscillation ocean dynamics: Simulation by coupled general circulation models. *Climate Dynamics: Why Does Climate Vary? Geophysical Monograph Series*, *189*, 53–64. https://doi.org/10.1029/2008gm000796

Capotondi, A., Ham, Y., Wittenberg, A., & Kug, J. (2015). *Climate model biases and El Niño Southern oscillation (ENSO) simulation*. US CLIVAR Variations. Retrieved from https://repository.library.noaa.gov/view/noaa/31041

Capotondi, A., & Sardeshmukh, P. D. (2017). Is El Niño *really* changing? *Geophysical Research Letters*, *44*(16), 8548–8556. https://doi.org/10.1002/2017gl074515

Capotondi, A., Wittenberg, A., & Masina, S. (2006). Spatial and temporal structure of Tropical Pacific interannual variability in 20th century coupled simulations. *Ocean Modelling*, *15*(3), 274–298. https://doi.org/10.1016/j.ocemod.2006.02.004

Capotondi, A., Wittenberg, A. T., Newman, M., Di Lorenzo, E., Yu, J.-Y., Braconnot, P., et al. (2015). Understanding ENSO diversity. *Bulletin of the American Meteorological Society*, *96*(6), 921–938. https://doi.org/10.1175/BAMS-D-13-00117.1

Caswell, T. A., Lee, A., Michael Droettboom, Elliott Sales de Andrade, Hoffmann, T., Klymak, J., et al. (2022). matplotlib/matplotlib: REL: v3.6.2 (Version v3.6.2). *Zenodo*. https://doi.org/10.5281/zenodo.7275322

Chen, C., Cane, M. A., Wittenberg, A. T., & Chen, D. (2017). ENSO in the CMIP5 simulations: Life cycles, diversity, and responses to climate change. *Journal of Climate*, *30*(2), 775–801. https://doi.org/10.1175/JCLI-D-15-0901.1

Chen, D., Lian, T., Fu, C., Cane, M. A., Tang, Y., Murtugudde, R., et al. (2015). Strong influence of westerly wind bursts on El Niño diversity. *Nature Geoscience*, *8*(5), 339–345. https://doi.org/10.1038/ngeo2399

Chiodi, A. M., & Harrison, D. E. (2013). El Niño impacts on seasonal US atmospheric circulation, temperature, and precipitation anomalies: The OLR-event perspective. *Journal of Climate*, *26*(3), 822–837. https://doi.org/10.1175/JCLI-D-12-00097.1

Chiodi, A. M., & Harrison, D. E. (2015). Global seasonal precipitation anomalies robustly associated with El Niño and La Niña events—An OLR perspective. *Journal of Climate*, *28*(15), 6133–6159. https://doi.org/10.1175/JCLI-D-14-00387.1

Collins, M., An, S.-I., Cai, W., Ganachaud, A., Guilyardi, E., Jin, F.-F., et al. (2010). The impact of global warming on the tropical Pacific Ocean and El Niño. *Nature Geoscience*, *3*(6), 391–397. https://doi.org/10.1038/ngeo868

Dai, A., & Wigley, T. M. L. (2000). Global patterns of ENSO-induced precipitation. *Geophysical Research Letters*, *27*(9), 1283–1286. https://doi.org/10.1029/1999gl011140

Deser, C., Phillips, A. S., & Alexander, M. A. (2010). Twentieth century tropical sea surface temperature trends revisited. *Geophysical Research Letters*, *37*(10), L10701. https://doi.org/10.1029/2010GL043321

European Centre for Medium-Range Weather Forecasts. (2019). *ERA5 reanalysis (0.25 degree latitude-longitude grid)*. Research Data Archive at the National Center for Atmospheric Research, Computational and Information Systems Laboratory. updated monthly. https://doi.org/10.5065/BH6N-5N20

Eyring, V., Bony, S., Meehl, G. A., Senior, C. A., Stevens, B., Stouffer, R. J., & Taylor, K. E. (2016). Overview of the coupled model intercomparison project phase 6 (CMIP6) experimental design and organization. *Geoscientific Model Development*, *9*(5), 1937–1958. https://doi.org/10.5194/gmd-9-1937-2016

Fedorov, A. V. (2002). The response of the coupled tropical ocean–atmosphere to westerly wind bursts. *The Quarterly Journal of the Royal Meteorological Society*, *128*(579), 1–23. https://doi.org/10.1002/qj.200212857901

Fedorov, A. V., Hu, S., Lengaigne, M., & Guilyardi, E. (2015). The impact of westerly wind bursts and ocean initial state on the development, and diversity of El Niño events. *Climate Dynamics*, *44*(5–6), 1381–1401. https://doi.org/10.1007/s00382-014-2126-4

Fredriksen, H., Berner, J., Subramanian, A. C., & Capotondi, A. (2020). How does El Niño–Southern Oscillation change under global warming—A first look at CMIP6. *Geophysical Research Letters*, *47*(22), e2020GL09064. https://doi.org/10.1029/2020gl090640

Gray, W. M. (1984). Atlantic seasonal hurricane frequency. Part I: El Niño and 30 mb Quasi-Biennial Oscillation influences. *Monthly Weather Review*, *112*(9), 1649–1668. https://doi.org/10.1175/1520-0493(1984)112<1649:ASHFPI>2.0.CO;2

Grothe, P. R., Cobb, K. M., Liguori, G., Di Lorenzo, E., Capotondi, A., Lu, Y., et al. (2019). Enhanced El Niño–Southern Oscillation variability in recent decades. *Geophysical Research Letters*, *47*(7), e2019GL083906. https://doi.org/10.1029/2019gl083906

Guilyardi, E., Wittenberg, A., Fedorov, A., Collins, M., Wang, C., Capotondi, A., et al. (2009). Understanding El Niño in Ocean–atmosphere general circulation models: Progress and challenges. *Bulletin of the American Meteorological Society*, *90*(3), 325–340. https://doi.org/10.1175/2008bams2387.1

Ham, Y.-G., & Kug, J.-S. (2012). How well do current climate models simulate two types of El Niño? *Climate Dynamics*, *39*(1–2), 383–398. https://doi.org/10.1007/s00382-011-1157-3

Harrison, D. E., & Giese, B. S. (1991). Episodes of surface westerly winds as observed from islands in the western tropical Pacific. *Journal of Geophysical Research*, *96*(S01), 3221–3237. https://doi.org/10.1029/90JC01775

Harrison, D. E., & Luther, D. S. (1990). Surface winds from tropical Pacific islands—Climatological statistics. *Journal of Climate*, *3*(2), 251–271. https://doi.org/10.1175/1520-0442(1990)003<0251:SWFTPI>2.0.CO;2

Hoerling, M. P. (2000). Understanding and predicting extratropical teleconnections related to ENSO. In *El Niño and the Southern Oscillation: Multiscale variability and global and regional impacts*.

Hoerling, M. P., & Kumar, A. (2002). Atmospheric response patterns associated with tropical forcing. *Journal of Climate*, *15*(16), 2184–2203. https://doi.org/10.1175/1520-0442(2002)015<2184:ARPAWT>2.0.CO;2

Horel, J. D., & Wallace, J. M. (1981). Planetary-scale atmospheric phenomena associated with the Southern Oscillation. *Monthly Weather Review*, *109*(4), 813–829. https://doi.org/10.1175/1520-0493(1981)109<0813:psapaw>2.0.co;2

Hoyer, S., Roos, M., Joseph, H., Magin, J., Cherian, D., Fitzgerald, C., et al. (2022). xarray. https://doi.org/10.5281/zenodo.6628513

Hu, S., Fedorov, A. V., Lengaigne, M., & Guilyardi, E. (2014). The impact of westerly wind bursts on the diversity and predictability of El Niño events: An ocean energetics perspective. *Geophysical Research Letters*, *41*(13), 4654–4663. https://doi.org/10.1002/2014gl059573

Huang, B., Thorne, P. W., Banzon, V. F., Boyer, T., Chepurin, G., Lawrimore, J. H., et al. (2017a). *NOAA extended reconstructed sea surface temperature (ERSST), version 5*. NOAA National Centers for Environmental Information. Obtained at NOAA/ESRL/PSD at their website. https://doi.org/10.7289/V5T72FNM

Huang, B., Thorne, P. W., Banzon, V. F., Boyer, T., Chepurin, G., Lawrimore, J. H., et al. (2017b). Extended reconstructed sea surface temperature, version 5 (ERSSTv5): Upgrades, validations, and intercomparisons. *Journal of Climate*, *30*(20), 8179–8205. https://doi.org/10.1175/JCLI-D-16-0836.1

Jin, F.-F., Kim, S. T., & Bejarano, L. (2006). A coupled-stability index for ENSO. *Geophysical Research Letters*, *33*(23), L23708. https://doi.org/10.1029/2006GL027221

Johnson, N. C., & Kosaka, Y. (2016). The impact of eastern equatorial Pacific convection on the diversity of boreal winter El Niño teleconnection patterns. *Climate Dynamics*, *47*(12), 3737–3765. https://doi.org/10.1007/s00382-016-3039-1

Kiladis, G. N., & Diaz, H. F. (1989). Global climatic anomalies associated with extremes in the Southern Oscillation. *Journal of Climate*, *2*(9), 1069–1090. https://doi.org/10.1175/1520-0442(1989)002<1069:GCAAWE>2.0.CO;2

Kim, S. T., Cai, W., Jin, F.-F., Santoso, A., Wu, L., Guilyardi, E., & An, S.-I. (2014). Response of El Niño sea surface temperature variability to greenhouse warming. *Nature Climate Change*, *4*(9), 786–790. https://doi.org/10.1038/nclimate2326

Kim, S. T., & Jin, F. F. (2011). An ENSO stability analysis. Part II: Results from the twentieth and twenty-first century simulations of the CMIP3 models. *Climate Dynamics*, *36*(7–8), 1609–1627. https://doi.org/10.1007/s00382-010-0872-5

Kim, S. T., & Yu, J. Y. (2012). The two types of ENSO in CMIP5 models. *Geophysical Research Letters*, *39*(11), L11704. https://doi.org/10.1029/2012GL052006

Kug, J.-S., Jin, F.-F., & An, S.-I. (2009). Two types of El Niño events: Cold tongue El Niño and warm pool El Niño. *Journal of Climate*, *22*(6), 1499–1515. https://doi.org/10.1175/2008jcli2624.1

Lee, T., & McPhaden, M. J. (2010). Increasing intensity of El Niño in the central-equatorial Pacific. *Geophysical Research Letters*, *37*(14), L14603. https://doi.org/10.1029/2010gl044007

Lengaigne, M., Guilyardi, E., Boulanger, J.-P., Menkes, C., Delecluse, P., Inness, P., et al. (2004). Triggering of El Niño by westerly wind events in a coupled general circulation model. *Climate Dynamics*, *23*(6), 601–620. https://doi.org/10.1007/s00382-004-0457-2

L'Heureux, M. L., Takahashi, K., Watkins, A. B., Barnston, A. G., Becker, E. J., Di Liberto, T. E., et al. (2017). Observing and predicting the 2015/16 El Niño. *Bulletin of the American Meteorological Society*, *98*(7), 1363–1382. https://doi.org/10.1175/bams-d-16-0009.1

Li, G., Ren, B., Yang, C., & Zheng, J. (2010). Indices of El Niño and El Niño Modoki: An improved El Niño Modoki index. *Advances in Atmospheric Sciences*, *27*(5), 1210–1220. https://doi.org/10.1007/s00376-010-9173-5

Lin, I.-I., Camargo, S. J., Patricola, C. M., Boucharel, J., Chand, S., Klotzbach, P., et al. (2020). ENSO and tropical cyclones. In *El Niño Southern Oscillation in a changing climate*. Wiley. https://doi.org/10.1002/9781119548164.ch17

Lloyd, J., Guilyardi, E., Weller, H., & Slingo, J. (2009). The role of atmosphere feedbacks during ENSO in the CMIP3 models. *Atmospheric Science Letters*, *10*(3), 170–176. https://doi.org/10.1002/asl.227

Ma, L., & Jiang, Z. (2021). Sensitivity of ENSO simulation to the convection schemes in the NESM3 climate system model: Atmospheric processes. *Frontiers of Earth Science*, *9*, 596442. https://doi.org/10.3389/feart.2021.596442

Magee, A. D., & Kiem, A. S. (2020). Using indicators of ENSO, IOD, and SAM to improve lead time and accuracy of tropical cyclone outlooks for Australia. *Journal of Applied Meteorology and Climatology*, *59*(11), 1901–1917. https://doi.org/10.1175/JAMC-D-20-0131.1

Maher, N., Matei, D., Milinski, S., & Marotzke, J. (2018). ENSO change in climate projections: Forced response or internal variability? *Geophysical Research Letters*, *45*(20), 11390–11398. https://doi.org/10.1029/2018gl079764

Marjani, S., Alizadeh-Choobari, O., & Irannejad, P. (2019). Frequency of extreme El Niño and La Niña events under global warming. *Climate Dynamics*, *53*(9–10), 799–5813. https://doi.org/10.1007/s00382-019-04902-1

McPhaden, M. J., Freitag, H. P., Hayes, S. P., Taft, B. A., Chen, Z., & Wyrtki, K. (1988). The response of the equatorial Pacific Ocean to a westerly wind burst in May 1986. *Journal of Geophysical Research*, *93*(C9), 10589–10603. https://doi.org/10.1029/JC093iC09p10589

McPhaden, M. J., Zebiak, S. E., & Glantz, M. H. (2006). ENSO as an integrating concept in Earth science. *Science*, *314*(5806), 1740–1745. https://doi.org/10.1126/science.1132588

Neale, R. B., Richter, J. H., & Jochum, M. (2008). The impact of convection on ENSO: From a delayed oscillator to a series of events. *Journal of Climate*, *21*(22), 5904–5924. https://doi.org/10.1175/2008JCLI2244.1

Patricola, C. M., Camargo, S. J., Klotzbach, P. J., Saravanan, R., & Chang, P. (2018). The influence of ENSO flavors on western North Pacific tropical cyclone activity. *Journal of Climate*, *31*(14), 5395–5416. https://doi.org/10.1175/JCLI-D-17-0678.1

Patricola, C. M., Cassidy, D. J., & Klotzbach, P. J. (2022). Tropical Oceanic influences on observed global tropical cyclone frequency. *Geophysical Research Letters*, *49*(13), e2022GL099354. https://doi.org/10.1029/2022gl099354

Patricola, C. M., Chang, P., & Saravanan, R. (2016). Degree of simulated suppression of Atlantic tropical cyclones modulated by flavour of El Niño. *Nature Geoscience*, *9*(2), 155–160. https://doi.org/10.1038/ngeo2624

Patricola, C. M., O'Brien, J. P., Risser, M. D., Rhoades, A. M., O'Brien, T. A., Ullrich, P. A., et al. (2020). Maximizing ENSO as a source of western US hydroclimate predictability. *Climate Dynamics*, *54*(1), 351–372. https://doi.org/10.1007/s00382-019-05004-8

Philander, S. G. H. (1983). El Niño Southern Oscillation phenomena. *Nature*, *302*(5906), 295–301. https://doi.org/10.1038/302295a0

Picaut, J., & Delcroix, T. (1995). Equatorial wave sequence associated with warm pool displacements during the 1986–1989 El Niño–La Niña. *Journal of Geophysical Research*, *100*(C9), 18393–18408. https://doi.org/10.1029/95JC01358

Rasmusson, E. M., & Carpenter, T. H. (1982). Variations in tropical sea surface temperature and surface wind fields associated with the Southern Oscillation/El Niño. *Monthly Weather Review*, *110*(5), 354–384. https://doi.org/10.1175/1520-0493(1982)110<0354:vitsst>2.0.co;2

Richter, I. (2015). Climate model biases in the eastern tropical oceans: Causes, impacts and ways forward. *Wiley Interdisciplinary Reviews: Climate Change*, *6*(3), 345–358. https://doi.org/10.1002/wcc.338

Ropelewski, C. F., & Halpert, M. S. (1987). Global and regional scale precipitation patterns associated with the El Niño/Southern Oscillation. *Monthly Weather Review*, *115*(8), 1606–1626. https://doi.org/10.1175/1520-0493(1987)115<1606:GARSPP>2.0.CO;2

Seager, R., Cane, M., Henderson, N., Lee, D.-E., Abernathey, R., & Zhang, H. (2019). Strengthening tropical Pacific zonal sea surface temperature gradient consistent with rising greenhouse gases. *Nature Climate Change*, *9*(7), 517–522. https://doi.org/10.1038/s41558-019-0505-x

Seiki, A., Takayabu, Y. N., Yasuda, T., Sato, N., Takahashi, C., Yoneyama, K., & Shirooka, R. (2011). Westerly wind bursts and their relationship with ENSO in CMIP3 models. *Journal of Geophysical Research*, *116*(D3), D03303. https://doi.org/10.1029/2010JD015039

Takahashi, K., Montecinos, A., Goubanova, K., & Dewitte, B. (2011). ENSO regimes: Reinterpreting the canonical and Modoki El Niño. *Geophysical Research Letters*, *38*(10), L10704. https://doi.org/10.1029/2011gl047364

Tang, T., Luo, J.-J., Peng, K., Qi, L., & Tang, S. (2021). Over-projected Pacific warming and extreme El Niño frequency due to CMIP5 common biases. *National Science Review*, *8*(10), nwab056. https://doi.org/10.1093/nsr/nwab056

Timmermann, A., An, S.-I., Kug, J.-S., Jin, F.-F., Cai, W., Capotondi, A., et al. (2018). El Niño-Southern Oscillation complexity. *Nature*, *559*(7715), 535–545. https://doi.org/10.1038/s41586-018-0252-6

Trenberth, K. E. (1984). Signal versus Noise in the Southern Oscillation. *Monthly Weather Review*, *112*(2), 326–332. https://doi.org/10.1175/1520-0493(1984)112<0326:SVNITS>2.0.CO;2

Trenberth, K. E. (1997). The definition of El Niño. *Bulletin of the American Meteorological Society*, *78*(12), 2771–2777. https://doi.org/10.1175/1520-0477(1997)078<2771:tdoeno>2.0.co;2

Trenberth, K. E., & Stepaniak, D. P. (2001). Indices of El Niño Evolution. *Journal of Climate*, *14*(8), 1697–1701. https://doi.org/10.1175/1520-0442(2001)014<1697:lioeno>2.0.co;2

Van Oldenborgh, G. J., Philip, S. Y., & Collins, M. (2005). El Nino in a changing climate: A multi-model study. *Ocean Science*, *1*(2), 81–95. https://doi.org/10.5194/os-1-81-2005

Wang, G., Cai, W., & Santoso, A. (2020). Stronger increase in the frequency of extreme convective than extreme warm El Niño events under greenhouse warming. *Journal of Climate*, *33*(2), 675–690. https://doi.org/10.1175/jcli-d-19-0376.1

Waskom, M. L. (2021). seaborn: Statistical data visualization. *Journal of Open Source Software*, *6*(60), 3021. https://doi.org/10.21105/joss.03021

Watanabe, M., Chikira, M., Imada, Y., & Kimoto, M. (2011). Convective control of ENSO simulated in MIROC. *Journal of Climate*, *24*(2), 543–562. https://doi.org/10.1175/2010jcli3878.1

Weng, H., Ashok, K., Behera, S. K., Rao, S. A., & Yamagata, T. (2007). Impacts of recent El Niño Modoki on dry/wet conditions in the Pacific rim during boreal summer. *Climate Dynamics*, *29*(2–3), 113–129. https://doi.org/10.1007/s00382-007-0234-0

Williams, I. N., Pierrehumbert, R. T., & Huber, M. (2009). Global warming, convective threshold and false thermostats. *Geophysical Research Letters*, *36*(21), L05702. https://doi.org/10.1029/2009GL039849

Williams, I. N., & Patricola, C. M. (2018). Diversity of ENSO events unified by convective threshold sea surface temperature: A Nonlinear ENSO index. *Geophysical Research Letters*, *45*(17), 9236–9244. https://doi.org/10.1029/2018gl079203

Wu, X., Deng, L., Song, X., Vettoretti, G., Peltier, W. R., & Zhang, G. J. (2007). Impact of a modified convective scheme on the Madden-Julian oscillation and El Nino–Southern Oscillation in a coupled climate model. *Geophysical Research Letters*, *34*(16), L16823. https://doi.org/10.1029/2007GL030637

Yang, C., & Giese, B. S. (2013). El Niño Southern Oscillation in an ensemble ocean reanalysis and coupled climate models. *Journal of Geophysical Research: Oceans*, *118*(9), 4052–4071. https://doi.org/10.1002/jgrc.20284

Yeh, S.-W., Kug, J.-S., & An, S.-I. (2014). Recent progress on two types of El Niño: Observations, dynamics, and future changes. *Asia-Pacific Journal of Atmospheric Sciences*, *50*(1), 69–81. https://doi.org/10.1007/s13143-014-0028-3

Yeh, S.-W., Kug, J.-S., Dewitte, B., Kwon, M.-H., Kirtman, B. P., & Jin, F.-F. (2009). El Niño in a changing climate. *Nature*, *461*(7263), 511–514. https://doi.org/10.1038/nature08316

Yu, J.-Y., & Kim, S. T. (2010). Identification of central-Pacific and eastern-Pacific types of ENSO in CMIP3 models. *Geophysical Research Letters*, *37*(15), L15705. https://doi.org/10.1029/2010gl044082

Yu, S., & Fedorov, A. V. (2020). The role of westerly wind bursts during different seasons versus ocean heat recharge in the development of extreme El Niño in climate models. *Geophysical Research Letters*, *47*(16), e2020GL088381. https://doi.org/10.1029/2020GL088381

Zheng, X.-T., Hui, C., & Yeh, S.-W. (2018). Response of ENSO amplitude to global warming in CESM large ensemble: Uncertainty due to internal variability. *Climate Dynamics*, *50*(11–12), 4019–4035. https://doi.org/10.1007/s00382-017-3859-7

Zheng, X.-T., Xie, S.-P., Lv, L.-H., & Zhou, Z.-Q. (2016). Intermodel uncertainty in ENSO amplitude change tied to Pacific Ocean warming pattern. *Journal of Climate*, *29*(20), 7265–7279. https://doi.org/10.1175/jcli-d-16-0039.1

Zuidema, P., Chang, P., Medeiros, B., Kirtman, B. P., Mechoso, R., Schneider, E. K., et al. (2016). Challenges and prospects for reducing coupled climate model SST biases in the eastern tropical Atlantic and Pacific oceans: The US CLIVAR Eastern Tropical Oceans Synthesis Working Group. *Bulletin of the American Meteorological Society*, *97*(12), 2305–2328. https://doi.org/10.1175/bams-d-15-00274.1